Technical Notes

Microcooling Channel Effect on a Monopropellant Microelectromechanical System Thruster Performance

Jeongmoo Huh* and Sejin Kwon†
Korea Advanced Institute of Science and Technology, Daejeon 305-701, Republic of Korea

DOI: 10.2514/1.B36393

I. Introduction

As MICROELECTROMECHANICAL system fabrication technology advances, the aerospace industry, in pursuing smaller, faster, and cheaper satellites, sees several opportunities for effective satellite operations. Miniature satellites with 1–10 and 10–100 kg masses are called nanosatellites and microsatellites, respectively; and they offer the advantages of faster and cheaper operation. With formation flight using several small satellites, the revisit time can be drastically improved, and almost real-time Earth observation is expected to be possible in the near future. Maneuverability is required for the normal operation of miniature satellites, for which the development of a small-scale propulsion system is essential.

A micropropulsion system can operate by using electrical or chemical energy. Electrical propulsion can be distinguished as electrothermal, electrostatic, and electromagnetic propulsions. Resistojets and arcjets are typical electrothermal thrusters that use inert gas heated by electrical energy as a propellant. Two previous related studies [1,2] regarding this propulsion type have reported specific impulses of 90 and 127 s with a required power of 30 and 100 W for approximately 30 and 125 mN thrust generation, respectively. Electrostatic and electromagnetic microthrusters, such as pulsed plasma thrusters, field emission thrusters, radio-frequency ion thrusters, and Hall effect thrusters, operate with ionized propellant accelerated by electrical energy and have specific impulse ranges of 600–5000 s, consuming a power per unit thrust of 10–100 W/mN [3–6]. The specific impulses of these propulsion are substantially higher than those of chemical propulsion systems; however, electric propulsion is sometimes not compatible with very small satellites without adequate energy storage and power-conditioning equipment [1,3].

Chemical propulsion uses stored energy in the propellant and has a higher-energy density than electrical propulsion. Previous work using chemical propulsion reported a cold-gas microthruster [7,8], a monopropellant microthruster [9–11], a bipropellant microthruster [12,13], and a solid-propellant microthruster [14,15]. Cold-gas propulsion is the simplest system using chemical propulsion but has a low specific impulse. In contrast, bipropellant propulsion has the highest specific impulse but requires a complex system including the storage, supply, and control devices for two propellants. Solid-propellant propulsion is simple and has a moderate specific impulse but reignition and throttling are impossible, although they are essential for satellite maneuvering. These actions are possible in monopropellant propulsion, which also offers a simpler system than a bipropellant system and a higher specific impulse than that of cold-gas propulsion.

Most of the previous work related to monopropellant microthrusters has presented difficulties regarding sufficient propellant decomposition due to excessive heat loss in microscale. The necessity of additional heater installation in hydrogen peroxide microthrusters has been described by Kundu et al. [11] and Kuan et al. [16]. However, use of low-conductivity material (such as ceramics [17,18] and glass [9,10]) as opposed to the silicon material generally used in the MEMS fabrication process has been tested for better heat energy conservation. In addition, the use of blended propellant [9,19] with higher-enthalpy input has also been proven as a possible choice to compensate for the thermal energy loss and improve performance of the monopropellant microthruster. However, the brittleness and frangibility of these materials after exposure to sudden temperature variation sometimes create cracks in the chamber, and partially melted glass from the high chamber temperature in the blended propellant monopropellant thruster is left behind.

To solve this problem, adding cooling channels in the microthruster were considered in this study, and the effect of cooling channels on the monopropellant thruster's performance was determined before the cooling channel could be practically applied in a blended propellant test. Two microthrusters with and without cooling channels were fabricated with a photosensitive glass MEMS process. An experimental test was conducted by measuring the surface temperatures and thrust generation of the microthrusters to evaluate how the microcooling channel affected the cooling effectiveness and performance variation of the monopropellant microthruster.

II. Microthruster Design and Fabrication

Given that low thermal conductivity materials are useful for heat energy conservation, photosensitive glass was chosen as a fabrication material, which has the lowest thermal conductivity among the considered MEMS fabrication materials, including silicon, stainless steel, high-temperature cofired ceramic, and low-temperature cofired ceramic. Glass has a thermal conductivity approximately 100 times lower than that of silicon, and this characteristic aids in suppressing heat energy dissipation from the microthruster chamber and improves microthruster performance. In addition, glass is easily and inexpensively wet etched by hydrofluoric acid, and a high aspect ratio of approximately 20 can be manufactured. Moreover, glass is transparent and chemical resistant, both of which are desirable characteristics for a microreacting device.

The use of the green monopropellants of HAN (NH_3OHNO_3, 96.04 g/mol), ADN ($NH_4N(NO_2)_2$, 124.06 g/mol), and hydrogen peroxide (H_2O_2, 34.01 g/mol) was considered. HAN and ADN have been used as base substances for propellant blending and generally have higher specific impulses than that of hydrogen peroxide. However, these ionic propellants have high viscosity, which causes large pressure drops in the microscale flow. In addition, these propellants require an additional heater in the catalyst chamber for preheating to be decomposable by the catalyst. However, although the cold-start decomposition reaction may be insufficiently intense, hydrogen peroxide can be easily decomposed by the catalyst at room temperature, and it has a lower viscosity than the other

Received 12 July 2016; revision received 10 March 2017; accepted for publication 13 March 2017; published online 26 May 2017.

*Postdoctoral Researcher, Department of Aerospace Engineering, 373-1 Guseong-dong, Yuseong-gu; jmheo@kaist.ac.kr. Student Member AIAA.

†Professor, Department of Aerospace Engineering, 373-1 Guseong-dong, Yuseong-gu; trumpet@kaist.ac.kr. Member AIAA.

green propellants. Therefore, hydrogen peroxide was chosen as both the monopropellant and the coolant in the cooling channels.

Given the required thrust range from 6 μN to 270 mN for nanosatellite operations [20], the target thrust was determined to be 50 mN for applications in the 10-kg-class nanosatellite maneuvering, including attitude control, orbit transfer, and orbit compensation. Considering previous work on a photosensitive glass microthruster [9], we designed the chamber pressure to be 2 bar. Under the chemical equilibrium assumption, the specific impulse was estimated to be 72 s at sea level (167 s at vacuum), and the required volume flow rate of the propellant was determined to be 3 ml/min. It is recommended that the injector design has a pressure drop of between 5 and 20% of the chamber pressure for stable thrust generation [21]. With the assumption of laminar flow through the microinjector, a 0.4 bar pressure drop was intended at the injector with a width, height, and length of 50, 350, and 500 μm, respectively. The catalyst chamber volume was designed using the catalyst capacity, which is the decomposable propellant mass flow rate divided by the catalyst specific volume. On the basis of the catalyst capacity of a previous study [22], a 1 g/scm^3 catalyst capacity was used for a platinum-coated alumina catalyst, and a 69 mm^3 catalyst chamber volume was required for the design propellant flow rate. Given the available photosensitive glass thicknesses, the catalyst chamber was designed with a width, height, and length of 3.5, 4.5, and 4.4 mm, respectively.

A converging and diverging conical nozzle was used for the acceleration of the decomposed gas. Under a one-dimensional isentropic flow assumption through the nozzle, the required nozzle throat area was estimated to be 0.329 mm^2 and the nozzle exit area was 0.331 mm^2 for the operation condition of a 2 bar chamber pressure and a 1 atm exit pressure. To ensure flow choking at the nozzle throat under the limitation of the fabrication accuracy of photosensitive glass wet etching, however, a 5 bar chamber pressure condition was considered to reduce the nozzle area, which had an area of 0.091 mm^2 for the nozzle throat and 0.13 mm^2 for the nozzle exit. Therefore, the required nozzle throat width and exit were 260 and 366 μm, respectively, as a two-dimensional profile in the plane of the 350 μm-thick available glass wafer. The contraction half-angle at the converging section was 45 deg, and the expanding half-angle at the diverging section was 12 deg, on the basis of the recommended angles considering microscale effects [23].

The cooling channel was designed to cool the structure by using a rectangular-shaped tube, which is generally considered to be a cooling channel geometry with a higher convection heat transfer possibility than that of other tube shapes such as a circle or triangle [24,25]. In addition, such a channel can also be easily fabricated through the glass wet-etching process. To determine the machinability of the designed microcooling channels, three different aspect ratio rectangular cross-section channels were fabricated with heights of 1, 0.5, and 0.3 mm and an identical width of 0.5 mm. The fabrication results showed that the long cantilevered structure of the channel was easily damaged during the wafer surface polishing process, but the square cross-section tube was still the most robust design among the three options. Therefore, the channels were designed as square tubes with a width of 0.5 mm and a height of 0.5 mm, covering the entire area of the microthruster chamber.

As a result, a microthruster with microcooling channels was designed with nine photosensitive glass wafers. To evaluate the performance variation caused by the channels, a microthruster without cooling channels was also designed by using the same number of wafers. The designed microthrusters are shown in Fig. 1.

The designed microthruster was fabricated with a photosensitive glass MEMS process. The designed thruster profile was first printed on a film mask; then, the mask was transferred to a chrome mask on a

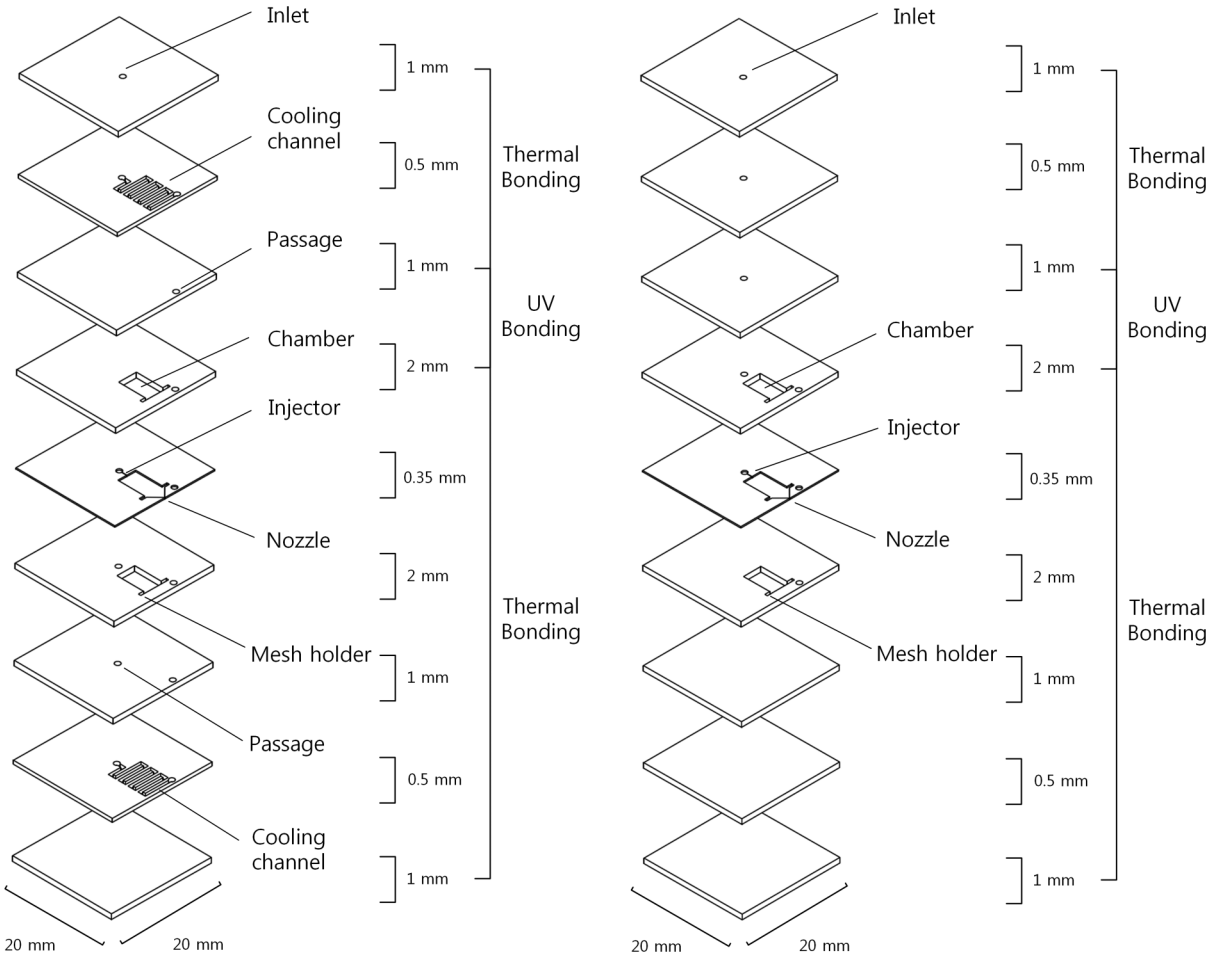

Fig. 1 Drawing of the designed microthrusters with (left) and without (right) cooling channels.

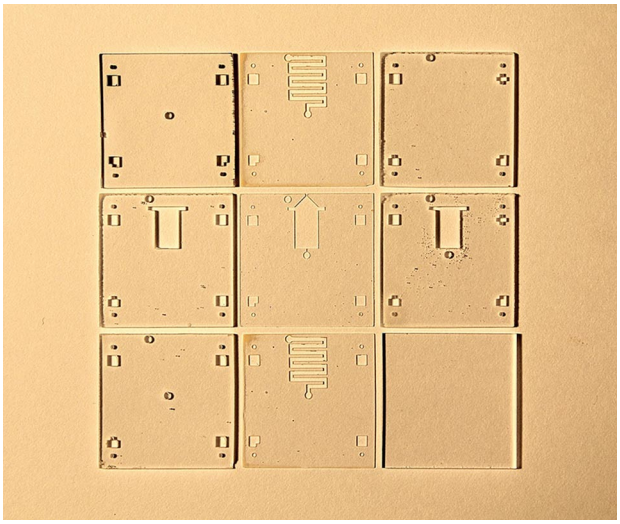

Fig. 2 Fabricated microthruster components on photosensitive glass wafers.

quartz wafer with photolithography. Photosensitive glasses were exposed to ultraviolet rays with a wavelength of 310 nm at 2.5 J/cm^2 with a chrome mask alignment for 30 s. After the UV exposure, the photosensitive glass was heat treated in a 585°C furnace for 45 min, and this was followed by wet etching. The UV exposed and thermally treated part of the photosensitive glass was wet etched by hydrofluoric acid 20 times faster than the unexposed part. In the wet-etching process, 10% hydrofluoric acid was used as the wet etchant, and the etching rate was approximately 10 $\mu m/$ min. The nine photosensitive glasses were surface polished before the bonding process. As shown in Fig. 1, both the thermal and UV bonding methods were used for the integration of all of the wafers. The microthruster components fabricated on nine photosensitive glasses are shown in Fig. 2. Enlarged images taken by optical microscopy of the microchannels with the injector and nozzle are shown in Fig. 3. The fabricated two-dimensional profile of the microchannels, injector, nozzle throat, and the nozzle exit had widths of 510.2, 49.8, 226.2, and 348.8 μm, as well as sufficient fabrication accuracies of 98, 99, 87, and 97%, respectively.

For the propellant decomposition, platinum-coated alumina was used as the catalyst, which has shown good performance with sufficient propellant decomposition efficiency in previous studies [9,10,22]. Through wet impregnation with a 10 wt % H_2PtCl_6 solution, the Pt was coated on the surface of the crushed alumina pellet with a 40–45 mesh size and dried in a convection oven. The fabricated catalyst was inserted into the thermally bonded microthruster chamber layers; then, the integration of the nine wafers was completed by UV bonding. The manufactured microthruster with cooling channels is shown in Fig. 4.

III. Experimental Testing and Discussion

The fabricated microthruster was experimentally tested by using 90 wt % hydrogen peroxide as a monopropellant, which has a 749°C adiabatic decomposition temperature, and it was purchased from HABO Chemical Technology Company, Ltd. The propellant was also used as the coolant in the cooling channels. The experimental setup comprised a thruster stand, a force transducer, a syringe, a syringe pump, Teflon tubes, valves, thermocouples, and data-acquisition equipment. For the thrust measurement, a model 9205 force transducer and 5015A charge meter manufactured by Kistler Company, Ltd. were used. The syringe and syringe pump were purchased from KD Scientific Company, Ltd. The 1/32 in. Teflon tubes and valves comprised the supply passage, which were made by the IDEX Health and Science Corporation. Open-tip k-type thermocouples measured the surface temperature of each side of the microthruster, and Kapton tape was used to firmly attach the thermocouples to the surfaces of the microthruster. The measured data were acquired with a data-acquisition system by National

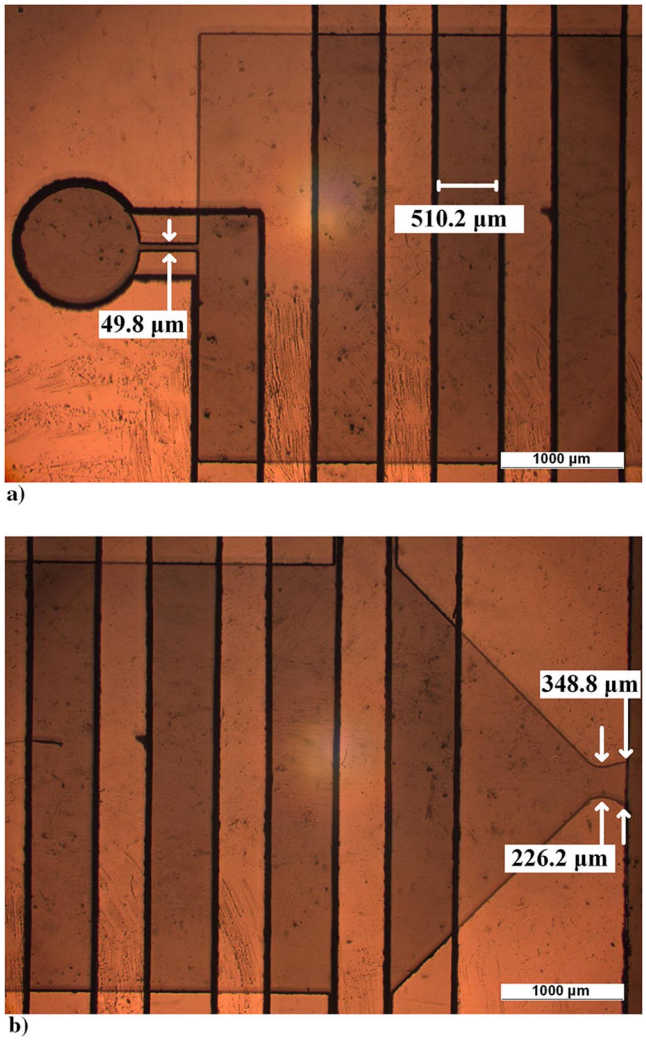

Fig. 3 Manufactured microcooling channels with a) injector and b) nozzle.

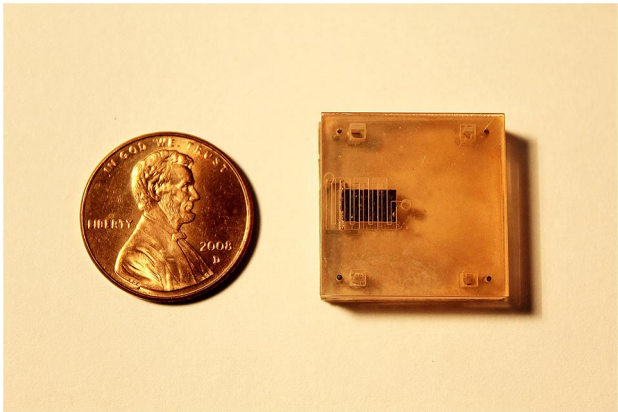

Fig. 4 Integrated microthruster with microcooling channels.

Instruments Company, Ltd. The experimental setup for the thrust measurement is shown in Fig. 5. The experimental testing of the microthruster was conducted in a dark room with a bright halogen lamp to visualize the invisible plume.

The experimental test results indicated the successful operation of the microthruster with performance repeatability, as shown in Fig. 6. Hydrogen peroxide was supplied by the syringe pump for 10 s for single pulse operation. After two cold-start pulse operations of the microthruster for chamber preheating, three pulse operations were recorded as shown in Fig. 7, which presents the measured thrust

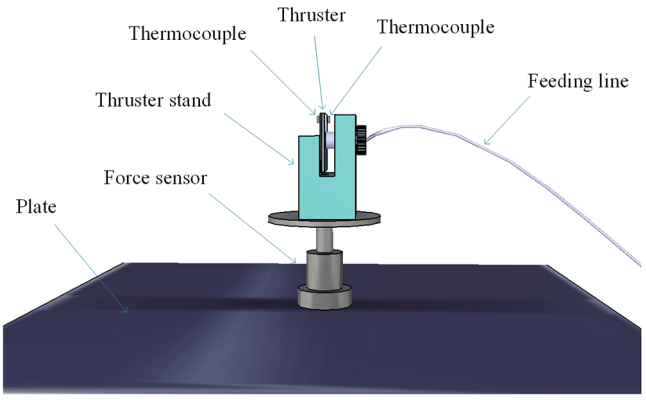

Fig. 5 Experimental setup for the microthruster performance test.

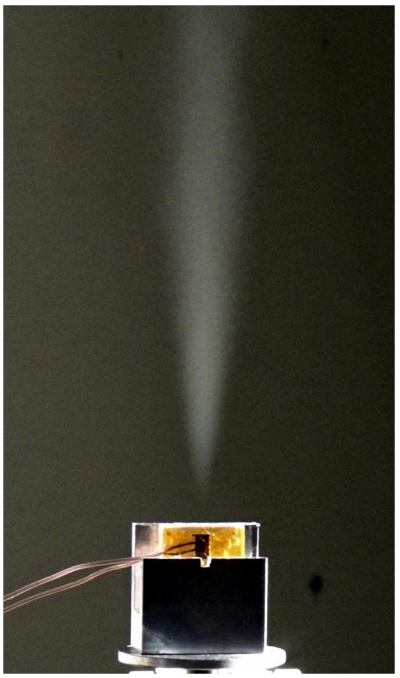

Fig. 6 Firing of the microthruster with cooling channels.

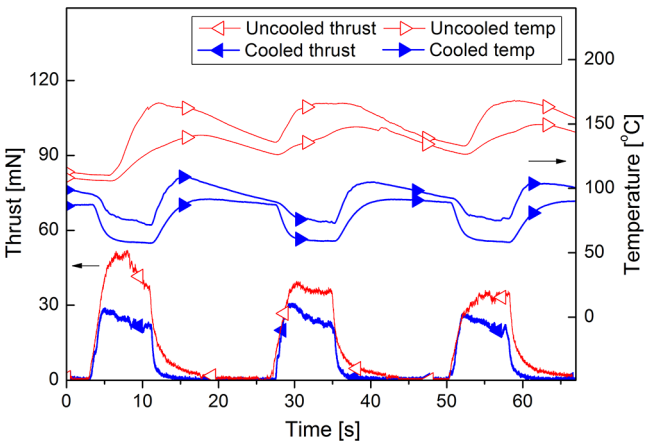

Fig. 7 Thrust and surface temperatures (temp) of the two microthrusters.

generation and surface temperatures of the two microthrusters. For the microthruster with microcooling channels, the surface temperatures decreased at the start of each pulse operation and maintained steady values during operation. Owing to the multiple pulse operations before data acquisition, the initial average surface temperature of the cooled thruster was 90°C, and the average surface temperature during operation was 65°C, thus presenting a 25°C temperature decrease. The maximum temperature of the cooled microthruster surfaces was 110°C, which occurred in the down time between the pulse operations of the thruster, owing to the absence of a cooling effect. The average peak thrust magnitude during the three pulse operations was 28.2 mN, with an average rising time of 3.7 s. In the uncooled microthruster without cooling channels, in contrast to the decreasing surface temperatures of the cooled microthruster, the surface temperatures increased at the start of each pulse operation and reached a maximum temperature at the end of each pulse operation. The initial average surface temperatures was 110°C and increased to 154°C, showing a temperature rise of 44°C. The maximum average temperature was approximately 165°C. The average peak thrust generation of the uncooled microthruster during the three pulse operations was 40.8 mN, which was higher than that of the cooled microthruster, and the average rising time was 4.2 s.

The performance test results showed the normal operation of the two photosensitive glass microthrusters with and without microcooling channels. With the microcooling channels, the average surface temperatures during operation were lower than that of the uncooled microthruster by as much as 89°C, which was a 58% decrease as compared to the uncooled average surface temperatures, thus demonstrating the successful cooling effect of the microcooling channels. The surface temperature changes between the initial and steady state temperatures during operation were −25°C for the cooled microthruster and +44°C for the uncooled microthruster, showing a 43% decrease in temperature due to use of the cooling channels. However, despite the supply of the same propellant flow rate, the thrust generation was decreased by 12.6 mN by use of the cooling channels, which was a 31% decrease from the value for the uncooled microthruster. The design specification and the experimental test result of the microthruster are summarized in Tables 1 and 2, respectively. The decreased thrust generation at the same propellant flow rate indicated a lower propellant decomposition efficiency due to the decreased catalyst reaction temperature caused by the cooling effect of the channels.

This result not only validates the effectiveness of the microcooling channels for microthruster structure cooling but also suggests the necessity of the consideration of the tradeoff between the cooling effect

Table 1 Summary of the microthruster design specification

Parameter	Value
Objective thrust	50 mN
Chamber pressure	2 bar
Specific impulse	72 s
Propellant/cooling fluid	90 wt % H_2O_2
Flow rate of H_2O_2	3 ml/ min
Catalyst	Pt/Al_2O_3
Catalyst support size	40–45 mesh
Catalyst capacity	1 g/scm^3
Convergent–divergent nozzle angle	45/12 deg
Cooling channel area	0.25 mm^2

Table 2 Summary of the microthruster experimental test

	Without cooling channels	With cooling channels
Objective thrust, mN	50	50
Designed specific impulse, s	72	72
Propellant flow rate, ml/ min	3	3
Thrust generation, mN	40.8	28.2
Initial temperature, °C	110	90
Average temperature ΔT, °C	154 (+44)	65 (−25)
Maximum temperature, °C	165	110
Rising time, s	4.2	3.7

and thruster performance, especially when the cooling channels are used in a monopropellant microthruster that has a catalyst chamber with a reaction rate affected by the surrounding temperature.

IV. Conclusions

As an alternative for the thermal management of fragile materials used for microthruster fabrication, the use of microcooling channels was considered and the effect of the cooling channels on microthruster performance was investigated. Two microthrusters were fabricated with and without cooling channels. The experimental test results showed differences in the thrust generation and temperature variation between the two microthrusters. The surface temperatures of the microthruster with microcooling channels successfully decreased during operation, and the average surface temperatures were lower than that of the uncooled thruster by as much as approximately 58%. However, the thrust generation also decreased by 31%, owing to the lower reaction temperature of the catalyst in the chamber. The experimental results indicated the normal operation of the two microthrusters and the effectiveness of the cooling channels applied to the glass structure for thermal management. There was, however, a decrease in performance due to the characteristics of monopropellant thruster, which has a catalyst in the chamber with a reaction rate that is affected by the surrounding temperature. Therefore, when cooling channels are used, especially in a monopropellant microthruster, additional considerations are required to address the tradeoff between the cooling effect and thrust generation.

Acknowledgments

This work was supported by the National Research Foundation of Korea (NRF) grant funded by the Korean government (MSIP) (no. NRF-2015R1A2A1A15055373).

References

[1] Leomanni, M., Garulli, A., Giannitrapani, A., and Scortecci, F., "Propulsion Options for Very Low Earth Orbit Microsatellites," *Acta Astronautica*, Vol. 133, No. 3, April 2017, pp. 444–454. doi:10.1016/j.actaastro.2016.11.001

[2] Haag, G. S., Sweeting, M. N., and Richardson, G., "Low Cost Propulsion Development for Small Satellites at the Surrey Space Centre," *13th Annual AIAA/USU Conference on Small Satellites*, Paper SSC99XII-2, Utah State Univ., Logan, UT, 1999.

[3] Sutton, G. P., and Biblarz, O., *Rocket Propulsion Elements*, 8th ed., Wiley, Hoboken, NJ, 2010, p. 663.

[4] Genovese, A., Tajmar, M., Buldrini, N., and Steiger, W., "2000-Hour Endurance Test of Indium Field Emission Electric Propulsion Microthruster Cluster," *Journal of Propulsion and Power*, Vol. 20, No. 2, 2004, pp. 219–227. doi:10.2514/1.9250

[5] Tajmar, M., and Scharlemann, C. A., "Development of Electric and Chemical Microthrusters," *International Journal of Aerospace Engineering*, Vol. 2011, March 2011, Paper 361215. doi:10.1155/2011/361215

[6] Charles, C., Boswell, R. W., Bish, A., Khayms, V., and Scholz, E. F., "Direct Measurement of Axial Momentum Imparted by an Electrothermal Radiofrequency Plasma Micro-Thruster," *Frontiers in Physics*, Vol. 4, 2016, Paper 19. doi:10.3389/fphy.2016.00019

[7] Kohler, J., Bejhed, J., Kratz, H., Bruhn, F., Lindberg, U., Hjort, K., and Stenmark, L., "A Hybrid Cold Gas Microthruster System for Spacecraft," *Sensors and Actuators A: Physical*, Vols. 97–98, April 2002, pp. 587–598. doi:10.1016/S0924-4247(01)00805-6

[8] Bayt, R. L., *Analysis, Fabrication and Testing of a MEMS-Based Micropropulsion System*, Massachusetts Inst. of Technology, Cambridge, MA, 1999, pp. 1–187.

[9] Huh, J., and Kwon, S., "Design, Fabrication and Thrust Measurement of a Micro Liquid Monopropellant Thruster," *Journal of Micromechanics and Microengineering*, Vol. 24, No. 10, 2014, Paper 104001. doi:10.1088/0960-1317/24/10/104001

[10] Lee, J., Kim, S., Kwon, S., and Yu, M., "Fabrication of Catalyst-Insertion-Type Microelectromechanical Systems Monopropellant Thruster," *Journal of Propulsion and Power*, Vol. 28, No. 2, 2012, pp. 396–404. doi:10.2514/1.B34287

[11] Kundu, P., Sinha, A. K., Bhattacharyya, T. K., and Das, S., "MnO_2 Nanowire Embedded Hydrogen Peroxide Monopropellant MEMS Thruster," *Journal of Microelectromechanical Systems*, Vol. 22, No. 2, 2013, pp. 406–417. doi:10.1109/JMEMS.2012.2226929

[12] Wu, M. H., and Lin, P. S., "Design, Fabrication and Characterization of a low-Temperature Co-Fired Ceramic Gaseous Bi-Propellant Microthruster," *Journal of Micromechanics and Microengineering*, Vol. 20, No. 8, 2010, Paper 085026. doi:10.1088/0960-1317/20/8/085026

[13] London, A. P., Ayon, A. A., Epstein, A. H., Spearing, S. M., Harrison, T., Peles, Y., and Kerrebrock, J. L., "Microfabrication of a High Pressure Bipropellant Rocket Engine," *Sensors and Actuators A: Physical*, Vol. 92, Nos. 1–3, 2001, pp. 351–357. doi:10.1016/S0924-4247(01)00571-4

[14] Oh, H.-U., Kim, T.-G., Han, S.-H., and Lee, J., "Verification of MEMS Fabrication Process for the Application of MEMS Solid Propellant Thruster Arrays in Space Through Launch and On-Orbit Environment Tests," *Acta Astronautica*, Vol. 131, Feb. 2017, pp. 28–35. doi:10.1016/j.actaastro.2016.11.013

[15] Liu, X., Li, T., Li, Z., Ma, H., and Fang, S., "Design, Fabrication and Test of a Solid Propellant Microthruster Array by Conventional Precision Machining," *Sensors and Actuators A: Physical*, Vol. 236, Dec. 2015, pp. 214–227. doi:10.1016/j.sna.2015.10.023

[16] Kuan, C. K., Chen, G. B., and Chao, Y. C., "Development and Ground Tests of a 100-Millinewton Hydrogen Peroxide Monopropellant Microthruster," *Journal of Propulsion and Power*, Vol. 23, No. 6, 2007, pp. 1313–1320. doi:10.2514/1.30440

[17] Cheah, K. H., and Low, K. S., "Fabrication and Performance Evaluation of a High Temperature Co-Fired Ceramic Vaporizing Liquid Microthruster," *Journal of Micromechanics and Microengineering*, Vol. 25, No. 1, 2015, Paper 015013. 10.1088/0960-1317/25/1/015013

[18] Wu, M. H., and Yetter, R. A., "A Novel Electrolytic Ignition Monopropellant Microthruster Based On Low Temperature Co-Fired Ceramic Tape Technology," *Lab on a Chip*, Vol. 9, No. 7, 2009, pp. 910–916. doi:10.1039/B812737A

[19] Lee, J., and Kwon, S., "Evaluation of Ethanol-Blended Hydrogen Peroxide Monopropellant on a 10 N Class Thruster," *Journal of Propulsion and Power*, Vol. 29, No. 5, 2013, pp. 1164–1170. doi:10.2514/1.B34790

[20] Janson, S. W., Helvajian, H., Hansen, W. W., and Lodmell, L. J., "Microthrusters for Nanosatellites," *2nd International Conference on Integrated Micro Nanotechnology for Space Applications (MNT99)*, Aerospace Corp., Pasadena, CA, April 1999.

[21] Huzel, D. K., and Huang, D. H., *Modern Engineering for Design of Liquid-Propellant Rocket Engines*, AIAA, Washington, D.C., 1992, p. 105.

[22] An, S., and Kwon, S., "Scaling and Evaluation of Pt/Al_2O_3 Catalytic Reactor for Hydrogen Peroxide Monopropellant Thruster," *Journal of Propulsion and Power*, Vol. 25, No. 5, 2009, pp. 1041–1045. doi:10.2514/1.40822

[23] Louisos, W. F., Alexeenko, A. A., Hitt, D. L., and Zilic, A., "Design Considerations for Supersonic Micronozzles," *International Journal of Manufacturing Research*, Vol. 3, No. 1, 2008, pp. 80–113. doi:10.1504/IJMR.2008.016453

[24] Wadel, M. F., "Comparison of High Aspect Ratio Cooling Channel Designs for a Rocket Combustion Chamber with Development of an Optimized Design," NASA Lewis Research Center TM-1998-206313, 1998.

[25] Cengel, Y. A., and Ghajar, A. J., *Heat and Mass Transfer: Fundamentals and Applications*, 4th ed., McGraw–Hill, New York, 2011, p. 437.

G. Richards
Associate Editor